ORIGINAL RESEARCH ARTICLE

Sintering Time Dependent Supersolidus Liquid Phase Sintering Behaviour of a Metal Injection Molded Nickel-Base Superalloy

ADDISON J. RAYNER and STEPHEN F. CORBIN

Supersolidus Liquid Phase Sintering of a high refractory metal Ni-based superalloy revealed that the liquid fraction and associated grain growth behaviour was dependent on the time at a given sintering temperature. This also led to a time dependence of part distortion and slumping. An existing SLPS model was modified to account for time dependent densification and distortion and compared to experimental measurements. Model and experimental agreement were very good and indicated no distortion after sintering at 1340 °C for 120 minutes, a transition to distortion after 30 to 45 minutes at 1345 °C and nearly immediate distortion at 1350 °C. These results indicate that a sintering time-temperature processing window can be defined where densification can be maximized without unwanted component distortion.

https://doi.org/10.1007/s11661-022-06734-x

I. INTRODUCTION

SUPERSOLIDUS liquid phase sintering (SLPS) has been successfully applied to difficult-to-sinter pre-alloyed powders to achieve high densities in short sintering time.[1–3] However, sintering a material above its solidus temperature reduces part strength and rigidity, which can lead to eventual part distortion and slumping if the incorrect SLPS conditions are employed.[2,3] The successful application of SLPS, therefore, requires a thorough understanding of the liquid behaviour with sintering time and temperature. To achieve both high density and shape retention in a given material, enough liquid must be present to enact densification while the liquid content is also kept low enough to avoid distortion. More specifically, the liquid film formed at the grain boundary during SLPS is critical because it can act as both a lubricant for grain sliding (which aids densification) and a source of grain cohesion *via* viscous resistance to deformation (which aids shape retention).[2,3] The application of SLPS is further complicated by the fact that optimal processing windows for densification and shape retention can vary significantly for different material conditions (*i.e.*, powder size and composition), with some materials exhibiting SLPS windows less than 10 °C wide.[1,4–6]

Although SLPS has been successfully applied to certain Ni-superalloys, such as metal injection molded (MIM) IN718,[5,7,8] more complex MIM Ni-superalloys containing higher levels of carbon and refractory metal (RM) elements are notably absent from the current body of SLPS literature. Compositionally modified Ni-superalloys with reduced levels of C and RM's such as Hf have been shown to exhibit significant grain growth,[9] though Ni-superalloys with standard levels of these elements do not always exhibit sub-solidus grain coarsening and can require supersolidus temperatures to experience grain growth.[10–13] Rayner and Corbin previously determined that it is possible to leverage the microstructural coarsening of SLPS to activate grain growth in a high RM MIM Ni-superalloy (NiSA).[14,15] In addition, the liquid content during SLPS was also found to be transient during isothermal hold time.[14,15] As the grain size and liquid content increases during SLPS, the grain boundary liquid film thickness increases, reducing the component's resistance to distortion.[2,3]

Numerous studies have been focused on modeling SLPS from first principles in order to predict the material response to time and temperature.[2,3,5,16–20] As a result of these works, there is a sound understanding of SLPS mechanisms and the research to date provides ample data and modeling approaches to predict and apply SLPS. However, current SLPS models do not consider the transient liquid behaviour discovered by Rayner and Corbin in a high RM MIM Ni-superalloy. The present work incorporates the transient liquid response of a high RM MIM Ni-superalloy into a generalized SLPS model. The MIM alloy in this study is a Ni-based superalloy containing Al, Co, Cr,

ADDISON J. RAYNER, and STEPHEN F. CORBIN are with the Dalhousie University, 1360 Barrington Street, Halifax, NS, B3H 4R2, Canada. Contact e-mail: Stephen.corbin@dal.ca
Manuscript submitted October 21, 2021; accepted May 16, 2022.
Article published online May 30, 2022

Ta, Ti, W and minor additions of other refractory metals (RMs), with the balance Ni (designated as NiSA). The SLPS model employed is based on the work of Campbell and Liu *et al.*[3,20] and serves as a qualitative model for SLPS behaviour. Though more realistic models are available in the literature,[16,17] the model from Campbell and Liu *et al.* serves as a more accessible approach to modeling general SLPS behavior.[3,20] Liu *et al.* comment on this, noting that the qualitative characteristics of the model agree with the expected response of real systems.[3] The successful application of this model to IN718 by Levasseur *et al.*[5] further confirms this conclusion.

The model presented by Liu *et al.* predicts the onset of densification and distortion based on the sintering temperature, liquid fraction, and physical properties of the alloy. The model also incorporates the influence of microstructural coarsening on the SLPS behaviour. The aim of the current work was to utilize differential scanning calorimetry (DSC) data in conjunction with the existing theory to model the SLPS behaviour of the NiSA with both time and temperature. Macroscopic observations of part rigidity as a function of sintering temperature and time were also completed to validate the new model predictions.

II. SLPS MODEL

Knowledge of the liquid volume and its distribution in the grain boundaries is critical to assess the rigidity of a material during SLPS. Liu *et al.* evaluated the rigidity of semi-solid structures during SLPS based on the liquid content and the extent of microstructural coarsening in the material.[3] The fractional grain coverage by liquid, F_c, can be expressed as[3,5,20]:

$$F_c = 2.64\left(\frac{V_L}{a}\right)^{1/2} \quad [1]$$

In Eq. [1], V_L is the liquid fraction present in the semi-solid structure and the parameter a is dependent on the dihedral angle, φ[3]:

$$a = \sqrt{3} + \frac{3}{\tan\left[30 - \left(\varphi/2\right)\right]} - \left[\frac{30 - \left(\varphi/2\right)}{60}\right] \cdot \left[\frac{\pi}{\sin^2\left[30 - \left(\varphi/2\right)\right]}\right] \quad [2]$$

The distribution of liquid throughout the grain boundaries is therefore dependent on the dihedral angle. In SLPS, the liquid volume fraction and dihedral angle are typically low and the idealized geometry exists for dihedral angles below 60 deg. This angle determines the stable neck size which forms between adjacent powder particles and is determined by the ratio of the solid–solid and solid–liquid interfacial energies, γ_{ss} and γ_{SL}, respectively.

The extent of solid bonds present in the structure can be defined in terms of contiguity, C_{SS}, which is dependent on the fractional grain coverage by liquid[3]:

$$C_{SS} = 1 - F_C \quad [3]$$

Contiguity can be used to determine the grain boundary film thickness, δ, of the liquid phase using the average grain size, G and the liquid and solid volume fractions V_L and V_S[3]:

$$\delta(1 - C_{SS}) = \frac{G}{3} \cdot \frac{V_L}{V_S} \quad [4]$$

Equation [4] states that the liquid film thickness increases as the grain size and liquid volume fraction increase. If the liquid film thickness increases, the resistance to movement between two grains, R, is decreased[3]:

$$R = \frac{\eta_L \upsilon A^2}{\delta^3} \quad [5]$$

In Eq. [5], η_L is the liquid viscosity, v is the relative velocity of two adjacent grains, and A is the grain face surface area. Therefore, the fractional grain coverage by liquid and liquid film thickness are dependent on the dihedral angle, average grain size, and liquid volume fraction. The dihedral angle is a physical constant for a given material, while the grain size and liquid fractions are variable with the processing conditions. The fractional grain coverage by liquid and the liquid film thickness both influence the structural rigidity of the material, and therefore play a role in controlling both densification and distortion.

Liu *et al.* derived a softening parameter, ζ, which combines multiple microstructural parameters to model the rigidity of the semi-solid structure during SLPS. An upper and lower bound on the SLPS process were defined as the onset of densification and onset of distortion[3]:

$$\zeta_{dens} = \left(\frac{\alpha\eta_L}{\sigma_{SS}}\right)^{1/3} \cdot \frac{(1 - C_{SS})^{1/5}}{(A - C_{SS})^{1/3}}; A = \frac{2.6\gamma_{LV}\cos\theta}{D\left(1 - \left(\rho_g/\rho\right)^{1/3}\right)} \cdot \frac{1}{\sigma_{SS}} \quad [6]$$

$$\zeta_{dist} = \left(\frac{\alpha\eta_L}{\sigma_{SS}}\right)^{1/3} \cdot \frac{(1 - C_{SS})^{5/3}}{(B - C_{SS})^{1/3}}; B = \frac{\rho g h}{2} \cdot \frac{1}{\sigma_{SS}} \quad [7]$$

$$\zeta = \frac{G^{1/3}}{3} \cdot \frac{V_L}{V_S}, \quad [8]$$

where α is a velocity constant, σ_{ss} is the strength of the solid–solid bonds, ρ_g is the green density, ρ is the instantaneous sintered density, D is the average particle size, and γ_{Lv} is the liquid-vapour surface energy. The onset of densification criterion in Eq. [6] is dependent on

the shear force between two grains overcoming the resistance to grain sliding.

Based on this criterion, there is a critical liquid film thickness, δ, at a given contiguity and grain size which will cause densification. The onset of distortion in Eq. [7] occurs when the force of gravity is greater than the resistance of the structure to deformation. This criterion is also satisfied at a critical liquid film thickness with a given contiguity and grain size. The generalized softening parameter, ζ, in Eq. [8] is dependent on the grain size and liquid fraction formed. The contiguity, which is dependent on the fractional grain coverage by liquid, is also encompassed in the model to reflect the microstructural characteristics during SLPS. Liu *et al.* also highlight that the upper and lower bounds of the densification and distortion are dependent on η_L, σ_{ss}, and C_{ss}, all of which are temperature dependent and none of which have a time dependence.[3]

III. EXPERIMENTAL METHODS

Rayner *et al.*[14] previously employed DSC to evaluate the SLPS behaviour of a MIM NiSA containing Al, Co, Cr, Ta, Ti, W and minor additions of other refractory metals (RMs), with the balance Ni (designated as NiSA). The reader is referred to the experimental methods described by Rayner *et al.*[14] for a detailed outline of that work.

MIM NiSA plates were prepared by an industrial partner and sent to Dalhousie University in the green-state. The green-state MIM plates were sectioned into smaller rectangular samples for DSC. The samples were 3.65 mm in height and were approximately 3.5 × 3.5 mm square. The top and bottom faces of the MIM plates were not altered to maintain a consistent sample height and good contact with the bottom of the DSC crucible. Thermal debinding was completed in a Sentrotech 1600C tube furnace under an argon gas atmosphere (99.999 pct Ar). A heating rate of 4.5 K/min was used and two isothermal debinding steps at both 180 °C and 850 °C were used in an inert powder support media. The debound samples were 57 pct of theoretical density after the debinding cycle.

De-bound MIM NiSA samples were analyzed using a Netzsch 404 F1 Pegasus DSC. The melting range of the MIM NiSA was previously determined to be 1270 °C to 1385 °C.[14] Samples were heated at 4.5 K/min under 50 mL/min flowing argon gas to SLPS temperatures of 1335 °C, 1340 °C, 1345 °C, and 1350 °C. Samples were isothermally held for 0, 15, 30, 60, and 120 minutes to measure the grain size over the SLPS hold time. A cooling rate of 20 Kpm was used and the furnace was evacuated and backfilled with argon gas prior to each test. Oxygen in the furnace atmosphere was removed using a zirconium getter ring place upstream of the sample.

Liquid fraction and average grain size data determined from earlier work[14] were applied in this study to determine their relationship with SLPS hold time and temperature. These relationships were then used as inputs to the outlined SLPS model from Liu *et al.*[3] with modifications that account for sintering time dependency.

Other important measurements carried out in the current study included performing stereomicroscopy and optical microscopy on the sintered samples to assess the degree of distortion and observe the bulk microstructure, respectively. The heights of post-sintered samples were also determined using an average of three caliper measurements to quantify the degree of height change and slumping during SLPS.

Note that in cases where multiple measurements were made, error bars or standard deviations are presented with the associated data set. The error bars represent the standard deviation of the data calculated using conventional methods.

IV. RESULTS

Stereomicroscopy of the SLPS samples was completed to determine the overall shape retention of the samples. The stereomicroscope images for a 15 and 120 minutes hold at temperatures of 1340 °C and 1350 °C are presented in Figures 1 and 2, respectively. The macro-scale images demonstrate the extent of slumping and deformation with increasing SLPS time and temperature. The 1340 °C samples retained their original shape over the 120 minutes hold time and some minor edge rounding was observable in the 120 minutes sample. The sample held for 15 minutes at 1350 °C was deformed to a much larger extent than the sample held for 120 minutes at 1340 °C. The sample held for 120 minutes at 1350 °C exhibited the largest amount of slumping and shape loss. The progressive shape loss with increasing hold time at a single temperature demonstrates one consequence of a transient liquid fraction during SLPS. In contrast, the samples held at 1340 °C demonstrate the ability of SLPS to achieve good shape retention below a critical liquid fraction.

Optical microscopy was also performed on the 1345 °C SLPS samples and polished cross sections showing the microstructures are presented in Figure 3. The cross sections in Figure 3 were etched with waterless Kalling's reagent and demonstrate the extent of sample

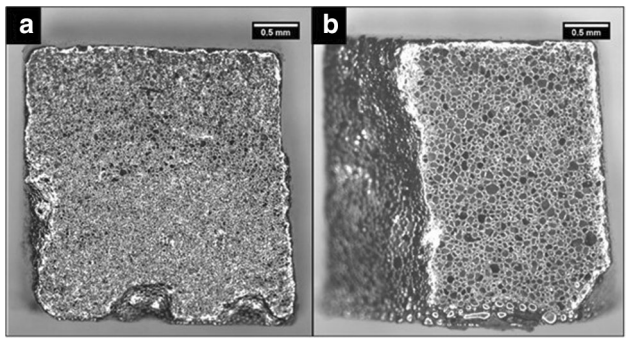

Fig. 1—Side-view stereomicroscope images of the MIM NiSA after being sintered at 1340 °C for (*a*) 15 min and (*b*) 120 min.

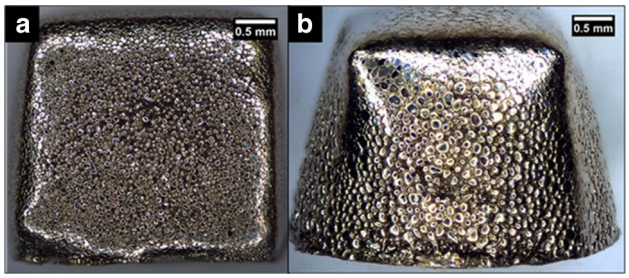

Fig. 2—Side-view stereomicroscope images of the MIM NiSA after being sintered at 1350 °C for (*a*) 15 min and (*b*) 120 min.

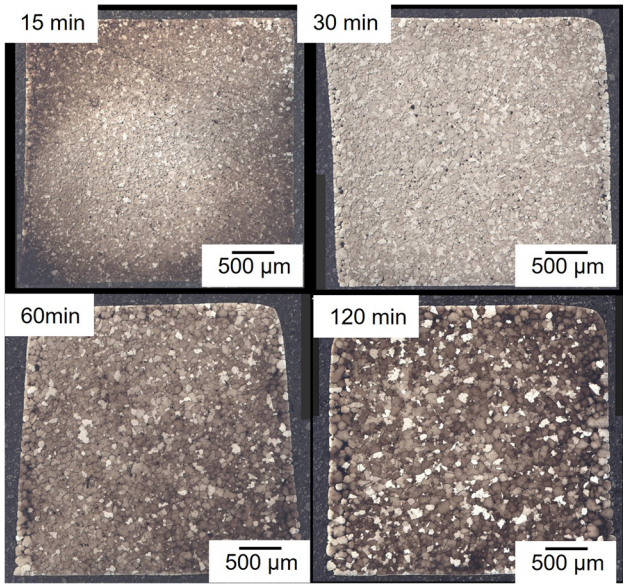

Fig. 3—Side-view of sample cross sections after SLPS at 1345 °C for 15, 30, 60 and 120 min hold times demonstrating the grain growth and slumping. Samples are oriented such that gravity is acting down.

deformation and the amount of grain growth over SLPS hold time.

The images of Figure 3 also indicate the time dependence of distortion, since the samples retained their shape at 15 minutes, experienced edge rounding at 30 minutes and exhibited some slumping and distortion at 60 and 120 minutes.

The height of the MIM NiSA samples were measured to assess the extent of slumping during SLPS and the results for each SLPS temperature are presented in Figure 4. The samples exhibit approximately 10 pct shrinkage during solid state sintering, which occurs during heating to the SLPS hold temperature. The samples are above 98 pct dense upon reaching 1345 °C and additional densification due to sintering shrinkage is limited. The 1340 °C and 1345 °C samples do not exhibit a significant decrease in height while the 1350 °C samples exhibit a steady loss of height over time. This result demonstrates that slumping occurs at the 1350 °C temperature.

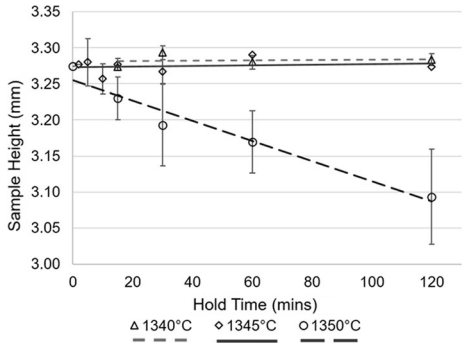

Fig. 4—Height measurements of the MIM NiSA after SLPS for different hold times.

V. ANALYSIS AND DISCUSSION

Rayner and Corbin previously determined that the liquid fraction and grain size in this NiSA are initially constant upon reaching the SLPS temperature of 1345 °C.[14,15] After an initial 10 minutes incubation period, both the liquid fraction and grain size were found to increase substantially. This dynamic response is important to model because the grain size and liquid fraction both influence the microstructure's liquid film thickness and resistance to distortion. . A power-law relationship was fitted to the 1345 °C data sets for both grain size and liquid fraction as it best described these data sets. The incubation period was taken into account by defining a fitted parameter, x_0, as 10.5 minutes to maximize the R^2 values and obtain the best fit. The experimental data employed to create the model equations was sourced from Rayner and Corbin[13,14] and is provided in Table I. The fitted equations with associated R^2 values are outlined in Eqs. [9] and [10]:

$$\text{Liquid Content (Pct)} = 18.99(x - x_0)^{0.0972};\ R^2 = 0.957 \quad [9]$$

$$\text{Grain Size } (\mu\text{m}) = 21.83(x - x_0)^{0.1699};\ R^2 = 0.997, \quad [10]$$

where x is the time at temperature in minutes and x_0 represents the fitted incubation time, 10.5 minutes. The data in Table I demonstrates that there is a significant increase in the liquid content over isothermal hold time once theincubation time is exceded. The dynamic nature of the liquid fraction beyond this threshold is caused by the solution of MC carbides and the subsequent time required for the NiSA to re-establish a stable equilibrium between the solid and liquid phases.[14,15] Previously developed SLPS models have not incorporated the time dependence of the liquid fraction due to relatively short times to reach equilibrium.[3,5] However, the NiSA in this study exhibits a sluggish segregation response to the solution of the MC carbides, taking over 50 minutes from the time of their dissolution to approach a new equilibrium liquid fraction.[14,15] Therefore, the time dependency of the liquid fraction must also be incorporated into the SLPS model for this NiSA.

Table I. Liquid Percentage, Grain Size and Density in the MIM NiSA During Isothermal Hold Time at 1345 °C With Initial 10 min Plateau. Data Sourced From Rayner *et al.* [14,15].

Hold Time, $(x-x_0)$ (Min)	Liquid (Pct)	Grain Size (μm)	Density (Pct)
− 10	18.6	17.4 ± 2.0	98.6 ± 0.3
− 8	18.6	18.4 ± 1.0	98.5 ± 0.3
− 5	17.9	20.8 ± 1.0	98.3 ± 0.3
0.5	17.5 ± 0.0	19.4 ± 1.0	98.7 ± 0.2
5	21.8 ± 3.2	28.7 ± 1.5	96.1 ± 0.3
20	27.0 ± 1.0	35.8 ± 2.8	97.6 ± 0.3
50	28.4 ± 0.5	43.9 ± 3.4	98.3 ± 0.4
110	28.4 ± 0.6	47.6 ± 3.4	98.4 ± 0.2

Table II. Parameters Used to Calculate the Onset Softening Parameters for Densification and Distortion

Viscosity ηL (mPa s)	Dihedral Angle φ (deg)	Wetting Angle θ (deg)	Surface Energy γLV (J)	Green Density ρg	Sintering Onset Density ρonset	Distortion Onset Density ρdist	Sample Height h (mm)
7.2[21]	35[2]	0[2]	1.5[2]	0.6	0.61	1	3.65

The SLPS grain size appears to be closely related to the liquid fraction given its similar power-law relationship with hold time (see Table I). Based on this observation, the grain coarsening of the MIM NiSA also exhibits a time dependency. Both the liquid fraction and grain size are dependent on temperature as well as time in the case of this NiSA, a feature that has not been reported in the literature for other SLPS PM superalloys.

To incorporate the time dependency of the liquid fraction and grain size into the existing SLPS model, the slope and exponent values for each function of time were plotted against temperature to determine the relationship between temperature and the power-law constants. These relationships were solved for the 1340 °C, 1345 °C, and 1350 °C SLPS temperatures to determine the power-law constants for the liquid fraction and grain size. These relationships represent the liquid fraction and grain size as a function of both time and temperature.

The generalized softening parameter was then calculated from Eq. [8] as a function of time and temperature using the experimentally determined grain size and liquid fraction relationships. The onset of densification and distortion were also calculated as function of time and temperature using Eqs. [6] and [7]. These equations were solved for σ_{ss} using the experimental value for ζ_{dens}, a viscosity of 7.2 mPas for liquid IN718 at 1336 °C,[21] a dihedral angle of 35 deg,[2] and a velocity constant of 3.3E5 m/s.[5] The physical parameters used in the model are outlined in Table II. The strength of the solid bonds was found to be 73.7 MPa which falls within the wide range of yield strengths reported for semi-solid systems.[2,5,22]

The modeled softening parameters over time at various SLPS temperatures are presented in Figures 5, 6 and 7. The curve derived from experimental results is

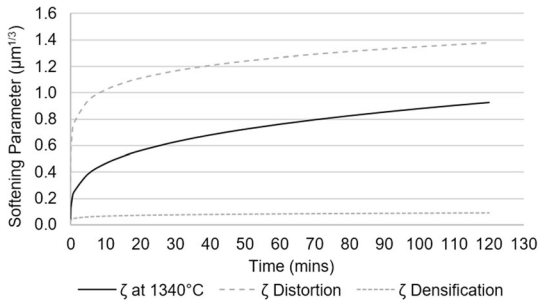

Fig. 5—Modeled softening parameter as a function of hold time at 1340 °C with the onsets of densification and distortion.

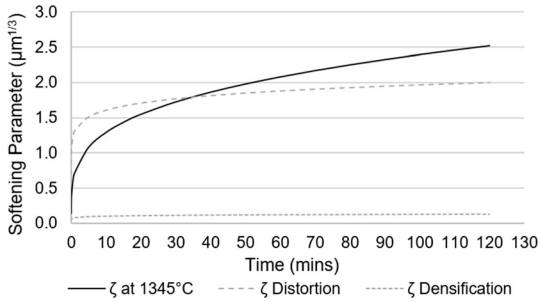

Fig. 6—Modeled softening parameter as a function of hold time at 1345 °C with the onsets of densification and distortion.

shown as a solid line. The evolving onset of distortion and densification predictions are also plotted against SLPS hold time as dashed lines and represent the upper and lower bounds of the SLPS process.

The predictions for the onset of densification is relatively constant over time and is lower than the predicted onset of distortion at all SLPS temperatures. The onset of distortion shows an initially rapid increase with SLPS time before reaching more steady values after

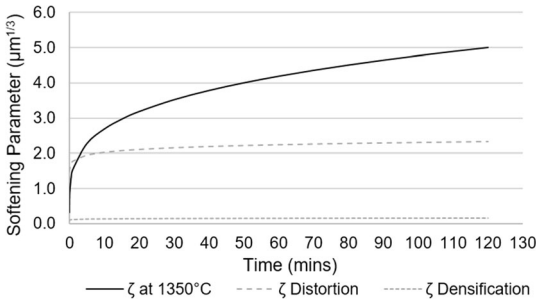

Fig. 7—Modeled softening parameter as a function of hold time at 1350 °C with the onsets of densification and distortion.

10 and 30 minutes. The upper and lower dashed onset lines represent the operating range of the SLPS process where densification will occur without distortion. This predicted operating range widens with increasing SLPS temperature.

The experimental softening parameter increases rapidly at the beginning of the SLPS process due to the increasing liquid fraction and grain size. It is important to remember that time zero in Figures 5 through 7 represents the time at which grain growth begins. The start of grain growth is associated with the solution of grain boundary MC carbides and occurs after approximately 10 minutes of hold time at the SLPS temperature of 1345 °C. Time zero was assumed to be at the same 10 minutes threshold for all modeled temperatures.

Once grain boundary MC carbides go into solution and the liquid fraction has increased, the alloy starts to approach a new equilibrium composition. As this occurs, the softening parameters trend toward a more steady state value.

The 1340 °C SLPS model in Figure 5 predicts that the NiSA will sinter within the operating range defined by the onset lines. The SLPS specimens of Figure 1 at this temperature exhibited densification without distortion, supporting the modeled results. At 1345 °C (see Figure 6), the softening parameter of the material rises faster than the onset of distortion, crossing above the upper bound after approximately 30 minutes (40 minutes of actual SLPS hold time and 30 minutes beyond the MC solution threshold). Based on this model, the material will retain its shape at SLPS hold times less than 40 minutes and lose its shape at times equal to or greater than 40 minutes at 1345 °C. The DSC specimens agree with the model, exhibiting no slumping or significant edge rounding in the 15 and 30 minutes hold tests and notable shape loss in the 60 and 120 minutes hold tests, as indicated in Figure 3. Although it is evident from the height data (see Figure 4) that there is no apparent slumping in the 1345 °C samples, there is clear evidence of edge rounding and bottom spreading with longer hold times in the polished cross sections (see Figure 3). This result is consistent with the modeled softening parameters presented in Figures 5 through 7 where some deformation is predicted beyond 40 minutes at 1345 °C and deformation is expected immediately upon reaching 1350 °C.

The model at 1350 °C (see Figure 7) predicts that the material will soften beyond the onset of distortion almost immediately upon exceeding the 10 minutes MC solution threshold. This was observed to be the case in the DSC specimens where none of the samples completely retained their shape (see Figure 2). Interestingly, the softening parameter in the 1350°C model continues to increase over the hold time, surpassing the distortion bound of the model by a factor of two by 120 minutes. The experimental results also confirmed this trend as the 1350°C samples were the only samples to slump (see Figure 4), decreasing in height under the weight of gravity after all hold times.

During the initial stages of SLPS for this MIM NiSA, grain boundary MC carbides are dissolved. After a critical threshold, dissolution of the MC carbides causes the liquid fraction to increase as the material progresses toward a new stable equilibrium liquid fraction. The microstructure also coarsens during this process, causing the grain size to increase along with the increasing liquid fraction. These trends are clear from the data sourced from Rayner and Corbin[14,15] (presented in Table I). Assuming the original powder particles densify quickly in the initial stages of SLPS, the following liquid fraction increase causes the grain boundary liquid film thickness to increase. The formation of additional liquid in the grain boundaries increases the fractional grain coverage by liquid according to Eq. [1], decreasing the contiguity and resistance to deformation as stated by Eqs. [3] and [5]. Therefore, the liquid fraction increase observed during SLPS causes the material's overall rigidity to decrease. In addition, the increasing liquid fraction and its distribution throughout the grain boundaries aids microstructural coarsening and grain growth. As grains grow at an isothermal SLPS temperature, the total grain boundary area is reduced leading to further increases in the grain boundary liquid film thickness, causing additional softening of the material.

The presented model is supported by the macroscopic results which exhibit deformation at times and temperatures above the predicted onset of distortion. Samples sintered at lower SLPS temperatures did not exhibit enough softening over the hold time to distort while higher temperature SLPS samples showed softening beyond the onset of distortion and were distorted. The continued softening of the higher temperature SLPS samples also corresponded with the observed microstructural coarsening with time at temperature. . In addition, each SLPS temperature would result in a separate equilibrium liquid fraction according to the phase equilibrium at the given peak temperature. This means that higher SLPS temperatures will result in larger softening parameters, a trend which is correctly captured by the model.

The liquid fraction and grain size relationships used in the presented model are plotted with the actual experimental data in Figures 8 and 9, respectively. The modeled liquid fraction behaviour exhibits good agreement with the measured liquid fractions for all three SLPS temperatures. The highest percent error between the modeled and experimental liquid fraction was 26 pct for 1345 °C/5 minutes while the lowest percent error was

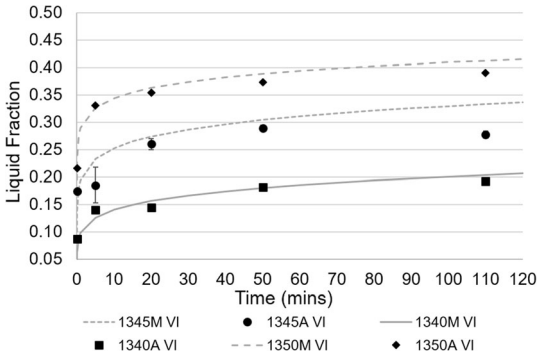

Fig. 8—Comparison of the modeled (“M”, lines) and actual (“A”, black markers) liquid fraction (Vl) over time for each SLPS temperature.

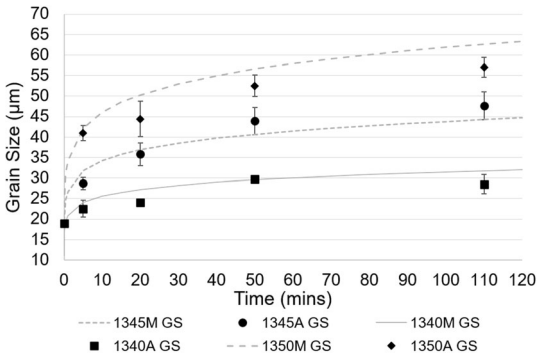

Fig. 9—Comparison of the modeled (“M”, lines) and actual (“A”, black markers) grain size (GS) over time for each SLPS temperature.

0.8 pct for 1340 °C/50 minutes. The modeled grain size also agrees with the measured grain sizes for all three SLPS temperatures. The highest percent error between the modeled and experimental grain size was 13 pct for 1350 °C/20 minutes while the lowest percent error was 0.5 pct for 1340 °C/50 minutes. The highest percent error for both parameters occurs during the first 20 minutes beyond the MC solution threshold, which is the most transient time period for the microstructure. However, the model and measured data sets show reasonable agreement overall, with the majority of the modeled behaviour exhibiting less than 10 pct error with the measured data for both liquid fraction and grain size.

The sluggish segregation response of the NiSA alloy to the solution of MC carbides complicates the SLPS process. For instance, sintering the NiSA alloy at 1340 °C for 60 minutes leads to a similar final liquid fraction than sintering at 1345 °C for 15 minutes with the same resulting grain size. However, sintering at 1345 °C for 60 minutes forms less liquid than 1350 °C for 30 minutes, but the resulting grain sizes are almost identical. The dynamic behaviour of the liquid fraction in this NiSA makes predicting these SLPS results challenging as both time and temperature influence the process to different extents *via* different mechanisms. The temperature determines the initial and final volume fractions of the solid and liquid phases as well as their equilibrium compositions. The temperature also controls the diffusion rates in the solid and liquid, the kinetics of MC carbide dissolution, and the liquid viscosity. The hold time controls the instantaneous liquid fraction and grain size, both of which determine the fractional grain coverage by liquid and the material’s overall rigidity.

Therefore, process designers require a comprehensive understanding of the material’s behaviour above the solidus temperature to practically apply SLPS to complex alloys such as this MIM NiSA. The SLPS model presented in this work captures the time-temperature dependency of the liquid fraction and grain size on the rigidity of the material, enabling a reasonable prediction of SLPS behaviour for a given time and temperature.

VI. CONCLUSIONS

The solution of grain boundary MC carbides during the initial stage of SLPS causes the liquid fraction to increase over an isothermal hold time. Simultaneous grain growth is aided by the transient liquid fraction, making grain size a function of time as well. Both the liquid fraction and grain size influence the material’s overall rigidity during SLPS, causing the softening of the material to be transient with time. Therefore, a modified SLPS model which incorporates the time dependency of these parameters above the solidus temperature was developed for the MIM NiSA. The behaviour of both the grain size and liquid fraction over time and temperature were incorporated into the accepted SLPS model to determine the instantaneous softening parameter of the material and onsets of both densification and distortion. The modeled results predict that no deformation will occur at 1340 °C for hold times under 120 minutes. The model also predicts that distortion will begin to occur after 40 minutes at 1345 °C and immediately upon MC carbide dissolution at 1350 °C. Macroscopic observations of shape retention support the modeled results, indicating that the modifications made to the model for this NiSA are appropriate. The results also illustrate the necessity for metallurgists to have thorough knowledge of an alloy’s behaviour above the solidus temperature when attempting to apply SLPS as a consolidation technique for geometry critical processes such as MIM.

ACKNOWLEDGMENTS

The authors would like to acknowledge the financial support received from the Natural Sciences and Engineering Research Council of Canada (NSERC) and Pratt and Whitney Canada (P&WC). Special thanks is given to Thomas Georges, Josianne Coulombe, and Orlando Scalzo for provision of materials for this research and useful technical discussions.

FUNDING

This study was funded by the Government of Canada under the Natural Sciences and Engineering Council and Pratt and Whitney Canada under the Industrial Research Chair program.

CONFLICT OF INTEREST

The research described in this paper was partially funded by Pratt and Whitney Canada (P&WC). The work was carried out with guidance and communication with P&WC personnel.

REFERENCES

1. R.M. German: *Sintering Theory and Practice*, Wiley, New York, 1996.
2. R.M. German: *Metall. Mater. Trans. A.*, 1997, vol. 28A, pp. 1553–67.
3. J. Liu, A. Lal, and R.M. German: *Acta Mater.*, 1999, vol. 47, pp. 4615–26.
4. K.A. Chuang and K.S. Hwang: *Metall. Mater. Trans. A*, 2011, vol. 42A, pp. 1896–1906.
5. D. Levasseur and M. Brochu: *Metall. Mater. Trans. A.*, 2016, vol. 47A, pp. 869–76.
6. Z.Y. Liu, N.H. Loh, K.A. Khor, and S.B. Tor: *Mater. Sci. Eng. A*, 2000, vol. 293, pp. 46–55.
7. J.L. Chan, J.R. Alcock, and D.J. Stephenson: *J. Mater. Sci.*, 1998, vol. 33, pp. 5131–36.
8. O. Ozgun, H.O. Gulsoy, R. Yilmaz, and F. Findik: *J. Alloys Compd.*, 2013, vol. 576, pp. 140–53.
9. N. Sheng, A. Meyer, K. Horke, C. Korner, and R.F. Singer: *Metall. Mater. Trans. A.*, 2020, vol. 52A, pp. 512–19.
10. G.H. Gessinger: Physical Metallurgy of Pre-alloyed Powders. in Powder Metall. Superalloys, Butterworth & Co., Cambridge, 1984, pp. 35–42.
11. M.F. Ashby and D.R.H. Jones: *Engineering Materials An Introduction to Their Properties and Applications*, Pergamon, Oxford, 1980.
12. A. Meyer, E. Daenicke, K. Horke, M. Moor, S. Müller, I. Langer, and R.F. Singer: *Powder Metall.*, 2016, vol. 59, pp. 51–56.
13. W.F. Smith: *Structure and Properties of Engineering Alloys*, 2nd ed. McGraw-Hill, New York, 1993.
14. A.J. Rayner and S.F. Corbin: *Mater. Today Commun.*, 2020, vol. 26, p. 101769.
15. A.J. Rayner: Ph.D. Thesis, Dalhousie University, 2020. http://hdl.handle.net/10222/78426.
16. S.P. Tucker and F.G. Hochgraf: *Metallography*, 1973, vol. 6, pp. 457–64.
17. M.F. Thorpe: *J. Non-Cryst. Solids*, 1983, vol. 53, pp. 355–70.
18. Y. Liu, R. Tandon, and R.M. German: *Metall. Mater. Trans. A.*, 1995, vol. 26A, pp. 2415–22.
19. Y. Liu, R. Tandon, and R.M. German: *Metall. Mater. Trans. A.*, 1995, vol. 26A, pp. 2423–30.
20. J. Campbell: *Metallography*, 1971, vol. 4, pp. 269–78.
21. J.J. Valencia, P.N. Quested: *Thermophysical Properties*. ASM Handbook. Casting, 2008, vol. 15, pp. 468–81.
22. M.C. Flemings: *Metall. Trans. B.*, 1991, vol. 22B, pp. 260–93.